**Atmospheric
Chemistry
and Physics
Discussions**

Interannual variation patterns of total ozone and temperature in observations and model simulations

W. Steinbrecht[1], B. Haßler[1], C. Brühl[2], M. Dameris[3], M. A. Giorgetta[4], V. Grewe[3], E. Manzini[5], S. Matthes[3], C. Schnadt[3,*], B. Steil[2], and P. Winkler[1]

[1]Meteorologisches Observatorium Hohenpeißenberg, Deutscher Wetterdienst, Hohenpeißenberg, Germany
[2]Chemie der Atmosphäre, Max Planck Institut für Chemie, Mainz, Germany
[3]Institut für Physik der Atmosphäre, Deutsches Zentrum für Luft und Raumfahrt, Oberpfaffenhofen, Germany
[4]Atmosphäre im Erdsystem, Max Planck Institut für Meteorologie, Hamburg, Germany
[5]Modellistica del Clima, Istituto Nazionale di Geofisica e Vulcanologia, Bologna, Italy
[*]now at: Institut für Atmosphäre und Klima, Eidgenössische Technische Hochschule, Zürich, Switzerland

Correspondence to: W. Steinbrecht (wolfgang.steinbrecht@dwd.de)

Title Page

Abstract | Introduction

Conclusions | References

Tables | Figures

|◄ | ►|

◄ | ►

Back | Close

Full Screen / Esc

Print Version

Interactive Discussion

EGU

Abstract

We report results from a multiple linear regression analysis of long-term total ozone observations (1979 to 2002, by TOMS/SBUV), of temperature reanalyses (1958 to 2002, NCEP), and of two chemistry-climate model simulations (1960 to 1999, by ECHAM4.L39(DLR)/CHEM (=E39/C), and MAECHAM4-CHEM). The model runs are transient experiments, where observed sea surface temperatures, increasing source gas concentrations (CO_2, CFCs, CH_4, N_2O, NO_x), 11-year solar cycle, volcanic aerosols and the quasi-biennial oscillation (QBO) are all accounted for. MAECHAM4-CHEM covers the atmosphere from the surface up to 0.01 hPa ($\approx$80 km). For a proper representation of middle atmosphere (MA) dynamics, it includes a parametrization for momentum deposition by dissipating gravity wave spectra. E39/C, on the other hand, has its top layer centered at 10 hPa ($\approx$30 km). It is targeted on processes near the tropopause, and has more levels in this region. Both models reproduce the observed amplitudes and much of the observed low-latitude patterns of the various modes of interannual variability, MAECHAM4-CHEM somewhat better than E39/C. Total ozone and lower stratospheric temperature show similar patterns. Main contributions to the interannual variations of total ozone and lower stratospheric temperature at 50 hPa come from a linear trend (up to 30 Dobson Units (DU) per decade, or -1.5 K/decade), the QBO (up to 25 DU, or 2.5 K peak to peak), the intensity of the polar vortices (up to 50 DU, or 5 K peak to peak), and from tropospheric weather (up to 30 DU, or 3 K peak to peak). Smaller variations are related to the 11-year solar cycle (generally less than 25 DU, or 2.5 K), and to ENSO (up to 15 DU, or 1.5 K). Volcanic eruptions have resulted in sporadic changes (up to -40 DU, or $+3$ K). Most stratospheric variations are connected to the troposphere, both in observations and simulations. At low latitudes, patterns are zonally symmetric. At higher latitudes, however, strong, zonally non-symmetric signals are found close to the Aleutian Islands or south of Australia. Such asymmetric features appear in the model runs as well, but often at different longitudes than in the observations. The results point to a key role of the zonally asymmet-

Title Page

Abstract | Introduction

Conclusions | References

Tables | Figures

◄ | ►|

◄ | ►

Back | Close

Full Screen / Esc

Print Version

Interactive Discussion

EGU

ric Aleutian (or Australian) stratospheric anti-cyclones for interannual variations at high-latitudes, and for coupling between polar vortex strength, QBO, 11-year solar cycle and ENSO.

1. Introduction

For many years, general circulation models (GCMs) have been major tools for atmospheric prediction. For weather forecasting, their time scales range from hours to days, for climate studies from years to decades (IPCC, 2001). On these longer time scales, decadal changes in radiatively active trace gases like H_2O, CO_2, O_3, $CFCs$, N_2O, and NO_x are important, particularly in the stratosphere (IPCC, 2001; WMO, 2003; Shine et al., 2003). For the investigation of stratospheric ozone depletion and its connection to climate change (WMO, 2003), many recent "chemistry-climate models" include a representation of atmospheric trace gases, their sources, sinks, and chemical reactions relevant for the stratosphere (Austin et al., 2003). Trace gases are transported throughout the model atmosphere. Their distributions change in space and time due to transport processes and photo-chemical reactions. Trace gas abundances are fed back into the radiation code of the model. Thus, changes in trace gases interactively couple back into dynamics and transport. This is essential for investigating connections between stratospheric ozone changes and climate change.

Climatologies and trends from stratospheric "chemistry-climate models" are realistic and have been validated (Hein et al., 2001; Austin et al., 2003; Manzini et al., 2003; Shine et al., 2003; Steil et al., 2003). The purpose of this study is to extend this climatological validation to the comparison of interannual variation patterns. In this sense, we "validate" two recent 40 year transient simulations by ECHAM4.L39(DLR)/CHEM, called E39/C hereafter (Dameris et al., 2005), and MAECHAM4-CHEM (Steil et al., 2003; Manzini et al., 2003). These simulations try to account for nearly all important sources of variance in the real atmosphere between 1960 and 2000. We compare typical modes and patterns of the interannual variations of total ozone and temperature

[ACPD](#)

5, 9207–9248, 2005

Interannual variations of total ozone and temperature

W. Steinbrecht et al.

Title Page

Abstract	Introduction
Conclusions	References
Tables	Figures

|◄ | ►|
◄ | ►

Back | Close

Full Screen / Esc

Print Version

Interactive Discussion

EGU

from these two model simulations, with those actually observed.

We follow the approach of Steinbrecht et al. (2003), which was based on a multiple linear regression analysis of near global long-term total ozone observations from satellite-based Total Ozone Monitoring Spectrometer (TOMS) and Solar Backscatter Ultra Violet (SBUV) instruments (Stolarski and Hollandsworth, 2003), and of temperature fields from NCEP reanalyses (Kistler et al., 2001). This provides global maps of interannual variation patterns of total ozone and lower stratospheric temperature (e.g. 50 hPa, or ≈22 km), correlated with the quasi-biennial oscillation of Equatorial zonal wind (QBO), with the 11-year cycle of solar activity, or with other influences. For observations and reanalyses, the results are the same as in Steinbrecht et al. (2003). However, now the same methodology can be applied to simulated total ozone and temperature fields from the two 40-year long model runs, and observed and modelled interannual variation patterns can be compared.

2. Data and method

2.1. Simulations and observations

The simulations were performed with two models derived from the European Center HAMburg version 4 (Roeckner et al., 1996), and the MA-ECHAM4 (Manzini and Bengtsson, 1996) general circulation models: ECHAM4.L39(DLR)/CHEM, called E39/C hereafter, and MAECHAM4-CHEM. Both are based on full coupling of the general circulation (GCM) model with the chemistry model CHEM (Steil et al., 1998). While the general circulation (GCM) part accounts for the meteorological processes, CHEM simulates the photochemistry relevant to stratospheric ozone, including heterogeneous chemistry. Trace gas concentrations from CHEM are fed back into the radiative scheme of the GCMs (Steil et al., 2003). For both simulations, the horizontal resolution used in the GCMs was the T30 truncation, and the mesh size for CHEM was $3.75° \times 3.75°$. In E39/C, 39 vertical model levels reach from the surface up to 10 hPa (30 km) (Dameris

et al., 2005), whereas in MAECHAM4-CHEM 39 model levels reach from the surface up to 0.01 hPa (80 km) (Steil et al., 2003; Manzini et al., 2003). With more levels near the tropopause, E39/C is targeted more on processes around the tropopause (Grewe et al., 2001; Schnadt et al., 2002; Schnadt and Dameris, 2003). MAECHAM4-CHEM, on the other hand, is a full troposphere-stratosphere-mesosphere model (Manzini and Bengtsson, 1996; Manzini et al., 2003). It includes better radiation and dissipation processes, especially momentum deposition by dissipating gravity wave spectra, which is parameterized in MAECHAM4-CHEM (Manzini and McFarlane, 1998), but not in E39/C. The two models also differ in their trace gas transport scheme: E39/C uses a semi-Lagrange method following Williamson and Rasch (1989), whereas MAECHAM4-CHEM uses the less diffusive SPITFIRE scheme (Rasch and Lawrence, 1998).

With both models, a simulation covering the 1960 to 1999 time period was carried out, with the same "transient" boundary conditions, i.e. realistically increasing chlorine and greenhouse gas concentrations ($CFCs$, CO_2, N_2O, CH_4, and NO_x; WMO, 2003), and observed variations in sea surface temperatures and ice-coverage (Rayner et al., 2003). Both simulations also included a nudged QBO (Giorgetta and Bengtsson, 1999), volcanic aerosol effects from the major eruptions in 1963, 1982, and 1991 (Timmreck et al., 2004), and spectral solar irradiation changes following the 11-year solar cycle. For the latter, 10.7 cm solar radio flux was converted to UV changes, as described in Lean et al. (1997). See also Tourpali et al. (2003). Details for the E39/C transient simulation, and the boundary conditions, are given in Dameris et al. (2005). The same boundary conditions were used for the MAECHAM4-CHEM run.

The subsequent analysis is based on gridded monthly mean data. For TOMS/SBUV we used the gridded version 7 data set on a 5°×10° latitude by longitude grid from Stolarski and Hollandsworth (2003), over the period from November 1978 to December 2000. Since TOMS and SBUV need sunlight for their measurements, no data are available in the polar regions in winter. NCEP reanalysis data are available throughout the year, on a 2.5°×2.5° grid (Kistler et al., 2001). Here we use NCEP data from January 1958 to December 2000, regridded to the TOMS/SBUV grid. The E39/C and

EGU

MAECHAM4-CHEM monthly means are on a $3.75° \times 3.75°$ grid, and cover the period from January 1960 to December 1999. For the analysis we use total ozone anomalies ΔO_3, and temperature anomalies ΔT at 50 and 400 hPa. Anomalies were derived by subtracting the climatological long-term monthly mean for the appropriate month of the
5 year and for each grid-cell from the actual monthly mean at each grid-cell.

2.2. Zonal mean anomalies

The long-term evolution of zonal mean anomalies, i.e. monthly mean anomalies averaged over all grid cells with the same latitude, for observations and model simulations, for total column ozone, for lower stratospheric temperature at 50 hPa ($\approx$22 km), and
10 for mid-tropospheric temperature at 400 hPa ($\approx$7 km), is given in Fig. 1. The largest interannual variations are found at high northern, and high southern latitudes, in the stratosphere. They are seasonally synchronized, and occur in winter and spring. Variations in the tropical and subtropical stratosphere are smaller, more regular, and less synchronized with season. The troposphere, generally, behaves less regular than the
15 stratosphere. Both model simulations give a similar picture to the observations and reanalyses.

However, the substantially lower 50 and 400 hPa temperatures before 1979 in the area south of 30°S in the NCEP reanalyses (blue colors in the left panels of Fig. 1) are not seen in the simulations. Before the introduction of global satellite observa-
20 tions in 1979, the observational basis was quite sparse in the Southern Hemisphere, particularly in the stratosphere. After 1979, this situation changed dramatically. This step is quite apparent in the NCEP reanalyses in Fig. 1 (see also Kistler et al., 2001). NCEP temperatures in the Southern Hemisphere are systematically higher after 1979 compared to before 1979, both in troposphere and stratosphere. We have to be very
25 careful, therefore, when using NCEP reanalysis data from the Southern Hemisphere before 1979. Nevertheless, except for trends, most of our results from the NCEP reanalysis were very similar, whether obtained for the 1979 to 2000 period, or for the 1958 to 2000 period.

[ACPD](#)

5, 9207–9248, 2005

Interannual variations of total ozone and temperature

W. Steinbrecht et al.

Title Page

Abstract	Introduction
Conclusions	References
Tables	Figures

◀ | ▶|

◀ | ▶

Back | Close

Full Screen / Esc

Print Version

Interactive Discussion

EGU

Interannual variations of total ozone and temperature

W. Steinbrecht et al.

A long term decline of total column ozone can be seen in the top panels of Fig. 1, by the change from red to blue colors. This decline is most pronounced at high southern latitudes, where the "Antarctic ozone hole" has been occuring since 1984. It is also large at northern latitudes, particularly in the 1990s. Compared to TOMS or the E39/C simulation, the ozone decline is more pronounced in the MAECHAM4-CHEM simulation. This is related to a general overestimation of total ozone in MAECHAM4-CHEM (Austin et al., 2003), and is discussed in Sect. 3.2. At the same time the stratosphere, e.g. at 50 hPa, has been getting colder. This cooling is most visible by the blue colors in the tropics after 1993. At high latitudes, interannual variations are very large, and Fig. 1 gives no clear indication for a cooling trend. From Fig. 1 it also seems that the troposphere might be warming, but this is more pronounced in the simulations. It is not very clear in the reanalyses. As mentioned, the low NCEP temperatures in the Southern Hemisphere before 1979 have to be treated with suspicion. Trends are discussed in Sect. 3.2.

In the stratosphere, the QBO, indicated by the black line near the Equator, shows a very clear influence on total ozone and 50 hPa temperature in tropics and sub-tropics. This is seen in observations/reanalysis and in both simulations. Phase changes of the QBO signal appear around 15° latitude, and possibly also around 50° to 60° latitude for 50 hPa temperature. The QBO signal is discussed in Sect. 3.3. While the QBO signal is, in general, quite visible, effects of the 11-year solar cycle (indicated by the black line near 90° N) are much less obvious, at least for the altitude levels shown in Fig. 1. One might see a tendency for higher total ozone and higher 50 hPa temperatures during solar maxima. See Sect. 3.4 for solar cycle effects.

Very pronounced warmings appear in 50 hPa temperature after the 3 major volcanic eruptions of 1963, 1982 and 1991. These warmings are generally larger in the simulations than in the reanalysis. This is discussed in Sect. 3.5. In the troposphere, QBO effects are essentially invisible. There, large effects of El Niño on 400 hPa temperature can be seen. During El Niño warm phases, i.e. negative excursions of the Southern Oscillation Index plotted near the Equator in the bottom panels of Fig. 1, temperatures

EGU

are above normal in the tropics and part of the extra-tropics. During La Niña cold phases, i.e. positive excursions of the plotted index, temperatures are lower. The simulations also reproduce the 400 hPa temperature anomalies quite reasonably. ENSO effects are discussed in Sect. 3.8.

5 2.3. Multiple linear regression

Figure 1 already gives a qualitative indication of different factors contributing to interannual and long-term variations of total ozone and temperature. In the following, we try to quantify these. From general knowledge about main influences on total ozone or lower stratospheric temperature (e.g. WMO, 2003), we assume a priori that only certain
10 main variations are important. Each is represented by a "predictor" time series, e.g. the QBO by Equatorial zonal wind anomalies, the 11-year solar cycle by solar radio flux at 10.7 cm, the El Niño/Southern Oscillation by the Southern Oscillation Index, and so on. An attribution to a few statistically significant main factors can be done by multiple linear regression. For each individual grid-cell, total ozone column anomalies ΔO_3, or
15 temperature anomalies ΔT, are described as a sum of predictor terms:

$$
\begin{aligned}
\Delta Y = {}& c_{TR}\, TR + c_{FS}\, FS + c_A\, A + c_{T(400)}\, T(400) \\
& + c_{QBO(10)}\, QBO(10) + c_{QBO(30)}\, QBO(30) \\
& + c_{u(60N)}\, u(60N) + c_{u(60S)}\, u(60S) \\
& + c_{ENSO}\, ENSO + \text{residual}
\end{aligned}
\tag{1}
$$

From a given time series ΔY at an individual grid cell, and from given influences, or "predictor" time series X, the coefficients c_X can be determined by a multiple linear least squares fit. The residual is, in general, an auto-correlated noise time series.
20 Here we neglect the noise autocorrelation, which is usually smaller than 0.5 in the tropics, and smaller than 0.3 outside of the tropics. The statistical significance level of our results might, therefore, be overestimated. For our purposes we use the predictor time series TR for a linear trend, 10.7 cm solar radio flux FS for the 11-year solar cycle, stratospheric aerosol optical depth A for stratospheric aerosol loading, $T(400)$

Interannual variations of total ozone and temperature

W. Steinbrecht et al.

Title Page

Abstract	Introduction
Conclusions	References
Tables	Figures

◀◀	▶▶
◀	▶
Back	Close

Full Screen / Esc

Print Version

Interactive Discussion

EGU

for tropospheric temperature (anomalies) at 400 hPa, Equatorial zonal wind anomalies at 10 and 30 hPa, QBO(10) and QBO(30), for the quasi-biennial oscillation, zonal wind anomalies at 60° latitude, 50 hPa, u(60N) and u(60S), as proxies for Polar Vortex strength, and the Southern Oscillation Index for the El Niño/Southern Oscillation

5 (ENSO) variation. See Steinbrecht et al. (2003) for details.

The regression according to Eq. (1) is carried out separately for each grid cell, and separately for the four seasons, northern winter (December, January, February), northern spring (March, April, May), northern summer (June, July, August), and northern fall (September, October, December). For each grid cell, and for the four seasons,

10 the different terms $c_X X$ then describe ozone, or temperature variations correlated with predictor X. As in Steinbrecht et al. (2003), a stepwise regression approach is used. The most important predictor is added first. Other predictors are tested and added later, if they are statistically significant at the, possibly overestimated, 90% confidence level of a partial F test. At each step, insignificant predictors are dropped. In the end,

15 only the most significant predictors remain in the Equation.

With the notable exception of T(400) and $ENSO$ in the tropics, the predictor time series are sufficiently orthogonal. The exclusion of the less significant predictors further reduces problems by allowing only one of two highly correlated predictors. In several tests, reducing the set of predictors gave very similar results for the remaining predic-

20 tors. For example, there was little difference in the results for solar cycle and QBO, whether polar vortex strength was added as predictor or not. Also, for various combinations of including or excluding T(400) and $ENSO$ as predictors, the results for the other predictors changed very little. Finally, we found that regression results change very little, whether data from the entire 1958 to 2000 period, or 1960 to 1999 for the

25 simulations, or the much shorter 1979 to 2000 period where used. To summarize, in our experience the regression gives generally very stable and consistent results.

EGU

3. Results

3.1. Variance described by regression

An important measure for the performance of a regression is R^2, the ratio of the variance described by the regression, i.e. the variance of all terms on the right side of Eq. (1), except for the residual, to the total variance, i.e. to the variance of the left side of Eq. (1). A perfect regression has $R^2 = 1$ and fully explains the total variance. Small $R^2 \approx 0$ indicates that the regression explains only a small part of the total variance. This can happen when random noise, atmospheric, or from a measurement, accounts for a large fraction of the total variance, or when important explanatory variables are missing.

For Fig. 2 and the following figures, we have chosen to select only one season, which presents a clear but typical example. If they appear important, differences in other seasons are mentioned. This approach is easier to digest and less confusing than to show many figures with results for all four seasons.

Examples for the global distribution of R^2 from the regression according to Eq. (1) are given for December/January/February in Fig. 2. Values of R^2 larger than about 0.6 indicate that the regression describes a major part of the variance. R^2 smaller than 0.4, however, indicates that the regression is not giving a good description. R^2 values are generally highest in winter and spring in the respective hemispheres, when variance is high, and are lower in summer and fall, when variance is low. The regression works best for total ozone (top panels), and slightly worse for stratospheric temperature at 50 hPa (middle panels). It works very poorly for tropospheric temperature at 400 hPa (bottom panels), with the exception of the tropical Pacific area.

Geographically, the regression works best for total ozone and 50 hPa temperature in the tropics, subtropics, and in polar regions. There is a substantial belt around 40° to 60° latitude, where R^2 is below 0.4 and the regression does a poor job. This belt is less pronounced in total ozone, more pronounced in 50 hPa temperature. It corresponds to the storm track and jet-stream regions, also to the region of breaking planetary

[ACPD](#)

5, 9207–9248, 2005

Interannual variations of total ozone and temperature

W. Steinbrecht et al.

Title Page

Abstract | Introduction

Conclusions | References

Tables | Figures

◀◀ | ▶▶

◀ | ▶

Back | Close

Full Screen / Esc

Print Version

Interactive Discussion

EGU

waves and to the edge of the polar vortex. Obviously, no simple predictor is included in Eq. (1) to account for such more complex phenomena. By using monthly mean data, non-linear phenomena like shorter life-time storms or jet-streams, breaking waves and shorter term variations of the polar vortex edge might be averaged out inappropriately.

⁵ However, over large areas of the globe, and for observations and simulations, the regression does give a surprisingly good description of total ozone and 50 hPa temperature variance, describing well over 60% of it. For MAECHAM4-CHEM, R^2 for total ozone is close to 1, and the regression describes variations almost perfectly in tropics, southern subtropics, and near the poles. In general we would expect the simulations to

¹⁰ be less noisy than observations. Therefore, the regression should work better for the simulations. However, this is not the case for E39/C total ozone, or for 50 hPa temperature from MAECHAM4-CHEM. The general patterns for observations and simulations are comparable, although there are differences. Near the Equator, for example, R^2 for 50 hPa temperature has a local minimum for the simulations, but not for NCEP

¹⁵ reanalysis.

3.2. Linear trend

Linear trends cofficients c_{TR} from Eq. (1), obtained for the 1979 to 2000 period for the observations, and for the 1978 to 1999 period for the simulations, are plotted in Fig. 3. Note that white areas in Fig. 3, and following figures, indicate that the trend

²⁰ term (or the respective terms in the following figures) was not statistically significant at the 90% confidence level. If we disregard the white, non-significant areas, observations and simulations show reasonably similar structures for the total ozone trends (top panels), but also some differences. The largest ozone trends are found at high latitudes, particularly in spring of the respective hemisphere. Trends for southern spring

²⁵ at high southern latitudes (not shown) are a bit larger, but look similar to the trends at high northern latitudes for northern spring in Fig. 3. Ozone decline is lowest in the tropics, where the observations even show a slight increase over the given period. This tropical ozone increase is not seen in the simulations. Qualitatively, how-

EGU

ever, both simulations reproduce the latitudinal structure of the observed ozone trend. The E39/C simulated total ozone trend is slightly smaller than observed, whereas the MAECHAM4-CHEM simulated trend is substantially too large. This comes from the fact that MAECHAM4-CHEM generally gives about 20% too high total column ozone, 5 because of too much downward transport and numerical diffusion in the lower stratosphere (Austin et al., 2003; Steil et al., 2003). Despite its more diffusive transport scheme, the additional levels near the tropopause reduce this problem substantially in E39/C (Grewe et al., 2002). Considering that MAECHAM4-CHEM gives 20% higher total ozone, it is not surprising to see larger ozone trends for the MAECHAM4-CHEM 10 simulation. When relative trends, % per decade, are considered, not absolute trends, Dobson Units (DU) per decade, as in Fig. 3, the quantitative agreement between observations and MAECHAM4-CHEM should be better. There are some differences in the longitudinally varying structures at high latitudes. For example, observations and MAECHAM4-CHEM simulation indicate the largest March/April/May total ozone trends 15 above Sibiria, whereas the E39/C simulation places them over the North Atlantic.

For 50 hPa temperatures, NCEP reanalysis and both simulations agree on substantial long-term cooling, by about 1 K/decade in a broad band from roughly 40° S to 40° N. Similar cooling is found in other seasons (not shown). At higher latitudes, the NCEP reanalysis indicates larger areas with statistically significant cooling than the simulations. 20 The E39/C simulation shows a latitudinally varying cooling/warming pattern above the North Atlantic/Asia that is not seen in NCEP reanalyis or the MAECHAM4-CHEM simulation.

As mentioned in Sect. 3.1, the regression explains only a small fraction of the tropospheric temperature variance. Nevertheless, Fig. 3 also shows temperature trends 25 at 400 hPa. Both simulations show significant warming at low latitudes by about 0.5 K/decade. This is not seen (or not significant) in the NCEP reanalyses. Interestingly, the E39/C simulation gives a tropospheric warming trend over North-Eastern Canada, that is also found in the NCEP reanalyses, whereas the MAECHAM4-CHEM simulation repoduces the tropospheric cooling around 80° S, 20° E that is seen in the

Title Page

Abstract | Introduction

Conclusions | References

Tables | Figures

◄ | ►

◄ | ►

Back | Close

Full Screen / Esc

Print Version

Interactive Discussion

EGU

NCEP data.

As mentioned in Steinbrecht et al. (2003), the observed temperature and ozone trends from Fig. 3 agree with results from other studies (Ramaswamy et al., 2001; Fioletov et al., 2002; WMO, 2003). The major part of the declining trend in total ozone must be attributed to increasing anthropogenic chlorine and bromine (WMO, 2003). Lower stratospheric cooling, on the other hand is attributed to decreasing lower stratospheric ozone levels, and to increasing CO_2 and water vapour (IPCC, 2001; WMO, 2003; Shine et al., 2003). Recently, chlorine levels seem to have begun decreasing in the stratosphere (WMO, 2003; Rinsland et al., 2003). It is now being discussed whether ozone might show signs of a beginning recovery (Newchurch et al., 2003; Steinbrecht et al., 2004). Unfortunately, the simulations have not yet been extended past 1999. This is planned for the near future, and should be very helpful for addressing questions about a beginning ozone recovery.

3.3. Quasi-Biennial Oscillation

Figure 4 shows the typical amplitude (valley to peak) of total ozone and temperature variations that are correlated with the QBO. Plotted is twice the standard deviation (i.e. 2σ) of the combined QBO time series term $c_{QBO(10)} QBO(10) + c_{QBO(30)} QBO(30)$. Since QBO winds at 10 and 30 hPa are nearly 90° out of phase, the use of the two QBO levels in Eq. (1) allows for an automatic adjustment of the QBO ozone or temperature signal to the proper phase. In Fig. 4, yellow and red colors indicate positive correlation between ozone or temperature anomalies and Equatorial wind anomalies at 30 hPa (i.e. high during westerly winds), whereas cyan and blue colors indicate inverse correlation (low during westerly winds).

The first thing to note in Fig. 4 is the remarkable similarity between the QBO variation patterns of total ozone and lower stratospheric temperature at 50 hPa. For each individual data set, i.e. for observations, MAECHAM4-CHEM, and E39/C simulation respectively, the two sub-panels look quite similar. 20 Dobson Units QBO-related ozone change seem to correspond to a 2 K QBO-related temperature change. During the

W. Steinbrecht et al.

Title Page

Abstract	Introduction
Conclusions	References
Tables	Figures

◀ | ▶|

◀ | ▶

Back | Close

Full Screen / Esc

Print Version

Interactive Discussion

[EGU](#)

QBO westerly phase (at 30 hPa) total ozone and 50 hPa temperature are above normal in the tropics, and are below normal in the sub-tropics. This is due to a QBO-induced secondary circulation (Baldwin et al., 2001). At the time of westerly winds at 30 hPa this secondary circulation decreases upwelling and adiabatic cooling of ozone poor air in the tropics, thereby increasing total ozone and warming the lower stratosphere (red belt at the Equator in Fig. 4). In the extratropics the secondary circulation decreases downwelling and adiabatic warming of ozone-rich air. This results in the blue regions of low total ozone and low 50 hPa temperature in the sub-tropics, in Fig. 4. Note that QBO effects are largest in the winter and spring hemisphere.

At latitudes equatorwards of 40°, both model simulations reproduce the observed QBO-related variations quite well. This has to be expected, since in both simulations the QBO in zonal wind is enforced by a nudging procedure (Giorgetta and Bengtsson, 1999). After nudging, the secondary meridional circulation of the QBO and the related effects in temperature and ozone column result from the simulated dynamics of the model (Giorgetta et al., 2002). E39/C shows a more pronounced QBO signal in 50 hPa temperature, and a less pronounced signal in total ozone. Probably, the higher temperatures result in increased chemical ozone destruction, and thus reduce the E39/C total ozone QBO signal.

Polewards of about 40° latitude, the zonal symmetry of the QBO-related patterns breaks down. There, regions with large amplitudes and with positive correlation of total ozone or temperature to 30 hPa QBO winds appear over the Labrador sea, or in a band reaching from the Mediterranean Sea to the Aleutians. This apparent phase change around 40° has been described, e.g. by Yang and Tung (1995). Despite obvious differences, the MAECHAM4-CHEM simulation reproduces these observed zonally non-symmetric patterns better than the E39/C simulation. Since QBO effects reach up to 1 hPa and above, it is not surprising that MAECHAM4-CHEM reacts in a more realistic way than E39/C, where the highest model level is around 10 hPa.

Although the QBO plays only a very minor role for tropospheric variations, plots for 400 hPa temperature anomalies correlated with the QBO have been included in Fig. 4.

In NCEP reanalyses and both simulations there are indications for higher 400 hPa temperatures in the tropics during the westerly phase of the QBO at 30 hPa. There are also some indications for similar extratropical features in NCEP reanalysis and the simulations, especially for MAECHAM4-CHEM.

3.4. 11-year solar cycle

Figure 5 shows the amplitude of variations correlated with the 11-year solar cycle. Again, total ozone and 50 hPa temperature show similar patterns. Generally, both models reproduce the observed amplitudes, in the equatorial region and summer (southern) hemisphere also the patterns. Total ozone and 50 hPa temperature are higher during solar maxima and lower during solar minima. At low and mid-latitudes, the amplitudes typically reach 5 to 10 DU or 0.5 to 1 K, and the patterns are zonally symmetric. Up to 30° or 40° latitude, the amplitudes increase with distance from the Equator. The ozone signal is similar in observations and simulations. The temperature signal is more pronounced in the NCEP reanalysis, less pronounced in the simulations.

Interestingly, solar cycle variations are largest, up to 30 DU or 3 K at high latitudes. These patterns are not zonally symmetric, and are found primarily near the polar vortices, and in winter and spring of the respective hemisphere, e.g. in December/January/February in the Northern Hemisphere (Fig. 5) and in September/October/November in the Southern Hemisphere (not shown). The meridional Brewer/Dobson circulation might transport the fairly large (5%) solar signal observed in low and mid-latitude upper stratospheric ozone (e.g. Newchurch et al., 2003; Steinbrecht et al., 2004) to certain regions near the winter poles. The simulations reproduce the large amplitudes of these zonally asymmetric high latitude patterns, but not their position. The simulated patterns are shifted to different longitudes.

Although the regression explains only a small part of tropospheric temperature variance at 400 hPa, we have included variations correlated with the solar cycle in the bottom panels of Fig. 5. Solar effects in the troposphere are minor and patchy, both in NCEP reanalyses and in the simulations. NCEP reanalyses show a band of posi-

Title Page

Abstract	Introduction
Conclusions	References
Tables	Figures

| ◄◄ | ►► |
| ◄ | ► |

| Back | Close |

Full Screen / Esc

Print Version

Interactive Discussion

EGU

tive temperature anomalies correlated with the solar cycle in the tropics, and several patches in the extra-tropics. Similar patterns are found in other seasons (not shown). Both simulations indicate an area of positive correlation in the tropics above Indonesia, and near the Aleutian tropospheric cyclone. This is remotely similar to the NCEP re-

5 analyses. Both simulations give negative correlation patches at southern mid-latitudes, whereas NCEP reanalyses have a negative pattern near sub-tropical South America. Although the tropospheric patterns are small and patchy, and agreement between models and observations is poor, Fig. 5 might hint at a relation between the solar cycle and tropospheric dynamics. See also the MAECHAM4-CHEM studies by Tourpali et al.

10 (2003, 2005) for tropospheric effects of the solar cycle.

3.5.   Volcanic aerosol

The magnitude of total ozone and temperature changes attributed to stratospheric aerosol from volcanic eruptions is given in Fig. 6. Different from the other figures, we have not plotted two standard deviations of the aerosol term $c_A A$, which consists of

15 three short spikes, but rather its minimum or maximum value. This minimum or maximum is usually reached in 1992 or 1993, after the 1991 eruption of Mt. Pinatubo. Thus, Fig. 6 usually gives the aerosol effect occuring after the Pinatubo eruption.

A major effect of the Pinatubo eruption was the large stratospheric warming due to enhanced aerosol (Robock, 2000). In a broad band around the Equator, the warming

20 exceeded 2 or 3 K for temperatures at 50 hPa (left panel, middle row of Fig. 6). In the model simulations the tropical warming is prescribed. The regression retrieves a very large tropical warming, up to 4.5 K, from the simulations. This is larger than found for the NCEP reanalyses (middle row), and indicates that the prescribed tropical volcanic warming is too strong (see also Fig. 1).

25 The volcanic response of the simulations at higher latitudes is not prescribed, but generated from by the model. Again, zonal symmetry is broken for the response to volcanic aerosol at high latitudes. The NCEP reanalyses extend the large tropical warming over North-America, i.e. east of the Aleutian stratospheric anti-cyclone, whereas

Title Page

Abstract   Introduction

Conclusions   References

Tables   Figures

◀   ▶

◀   ▶

Back   Close

Full Screen / Esc

Print Version

Interactive Discussion

EGU

EGU

the simulations extend it above Sibiria, west of the Aleutian stratospheric anti-cyclone.

In the E39/C simulation, the warming covers nearly the entire polar cap. An important aspect is that the E39/C simulation produces a mid-winter stratospheric warming in the winter 1992/93. This mid-winter warming does not occur in the observations/reanalyses, or in the MAECHAM4-CHEM simulation (compare Fig. 1). To a substantial degree, stratospheric winter warmings occur at random, both in reality and in simulations. Even for constant boundary conditions, it has to be expected that some model winters will have warmings, while other years will have no warmings. Therefore, the polar warming in the E39/C simulation in Fig. 6 could be a random effect and should not be interpreted as a systematic error of the E39/C simulation. See e.g. Timmreck et al. (2004) for more information about various ECHAM-based simulations of the Pinatubo aerosol cloud.

The 1992/93 mid-winter warming in the E39/C simulation also explains why this simulation has a positive total ozone response at high latitudes (upper panels of Fig. 6). This is quite different from the TOMS/SBUV observations and the MAECHAM4-CHEM simulation, which show large ozone losses, exceeding 30 DU, at high latitudes. At low latitudes ozone losses are much smaller, in both simulations. The TOMS/SBUV observations even give a slight increase in total ozone near the Equator. A substantial fraction of the large ozone losses at high latitudes comes from chemical destruction by chlorine, which is activated particularly at high latitudes in winter and spring on the greatly enhanced aerosol surface at low temperatures (Solomon et al., 1996; Robock, 2000; Timmreck et al., 2004). The ozone decrease at low latitudes in the models, comes from lifting of the ozone profile. Lifting is caused by the net-heating due to Pinatubo aerosol, which increased vertical ascent rates in the tropics (Stenke and Grewe, 2005). Note that ozone formation from high SO_2 immediately after the eruption is not considered in the simulations, but might explain the positive response seen near the Equator in the TOMS data.

In the troposphere (bottom panels), NCEP reanalysis and both simulations give patches of significant cooling by around 1 K at low latitudes. At higher latitudes there

are nearly no consistent tropospheric features between reanalyses and simulations.

3.6. Polar vortex strength

The intensity of the meridional residual Brewer-Bobson circulation in the winter strato-sphere is highly correlated with the strength of the polar winter vortex (Salby and
5 Callaghan, 2002). A strong vortex goes hand in hand with a weak meridional circu-lation. Less ozone and heat are transported polewards. Total ozone and temperatures remain high at lower latitudes and are low at higher latitudes. A strong and cold vortex also favors rapid chemical ozone destruction in spring ("ozone hole", e.g. Solomon, 1999), which will result in low total ozone and, through less ozone radiative heating,
10 also in lower 50 hPa temperatures. This enhances the transport effect. It is more rel-evant for the Northern Hemisphere where "ozone hole" conditions only occur in some years, than for the Southern Hemisphere, where a strong and stable vortex is estab-lished and an "ozone hole" forms in almost every year. In the regression, we use zonal wind anomalies at 60° latitude, 50 hPa level, as a proxy for vortex strength.
15   The size of total ozone and 50 hPa temperature fluctuations, correlated with zonal wind anomalies, is shown in Figs. 7 and 8 for northern and southern spring, respec-tively. Particularly in the Southern hemisphere, spring is the season when vortex strength effects are most pronounced. As expected, total ozone and 50 hPa tempera-tures in the polar region are inversely correlated with 60° zonal wind or vortex strength.
20 Polar ozone and temperature are low, when the vortex is strong. The polar variations are very large and reach up to 50 DU or 5 K. At low to mid latitudes, however, total ozone or 50 hPa temperature are high, when the vortex is strong and 60° zonal wind is high. The temperature variation is more pronounced and reaches to higher latitudes than the total ozone variation. Temperature variations peak at up to 2.5 K around 30° N
25 to 40° N. Total ozone variations are more restricted to the tropics and reach up to 5 or 10 DU. Both model simulations show similar, even more pronounced, patterns com-pared to the observations. The observed zonally asymmetric structure at high latitudes is matched well by MAECHAM4-CHEM, slightly less well by E39/C.

EGU

Interannual variations of total ozone and temperature

W. Steinbrecht et al.

In southern spring (September/October/November), however, E39/C does not reproduce the results of the observations, or of MAECHAM4-CHEM. We attribute this to the strong polar cold bias of E39/C (Austin et al., 2003). In E39/C the southern polar vortex remains too stable for too long, and the final warming occurs too late in the year, often
5 not before December. During September and October, the E39/C simulated southern vortex does not vary enough, and does not generate enough ozone and temperature variations for a significant signal in Fig. 8.

In general, the Southern Hemisphere variations are slightly weaker, especially in the tropics, than in the Northern Hemisphere. Results for northern vortex strength in
10 fall and winter (September/October/November, and December/January/February, all not shown), are very similar to northern spring, shown in Fig. 7. However, variations attributed to southern vortex strength in southern fall and winter (March/April/May, and June/July/August, all not shown), are much weaker than in southern spring, presented in Fig. 8. Probably, this reflects the much stronger and less variable Antarc-
15 tic vortex and the generally weaker Brewer-Dobson circulation in the Southern Hemisphere. An interesting aspect in Fig. 8 is the (blue) low 50 hPa temperature pattern above Northern Canada that is correlated with a strong southern vortex in September/October/November. It is found both in NCEP reanalyses and MAECHAM4-CHEM simulation. This might point to an interhemispheric connection, by which the ending
20 southern polar vortex is connected with the beginning northern polar vortex.

For completeness, we are also including the tropospheric 400 hPa temperature variation patterns in the lower panels of Figs. 7 and 8. Tropospheric temperature does show substantial correlation with stratospheric polar vortex strength. This is not new, and has been described extensively within the Annular Modes concept (Thompson and
25 Wallace, 2000). As shown e.g. by Baldwin and Dunkerton (1999) stratospheric polar vortex anomalies tend to propagate to lower atmospheric levels, and can sometimes reach down into the troposphere. In our investigation we find consistent patterns between NCEP reanalyses and both model simulations. In Fig. 7, a strong northern vortex is statistically correlated with low 400 hPa temperatures over the Labrador Sea, and

EGU

also over parts of the tropics, whereas higher temperatures occur in a band between 40° N and 60° N, e.g. over the Atlantic or Europe. Corresponding, more pronounced and more zonally symmetric patterns are found in Fig. 8 for the southern vortex and 400 hPa temperatures south of 40° S. As mentioned previously, these correlations account for only a small fraction of the total tropospheric variance. Nevertheless, it is reassuring to find them in reanalyses and both model simulations. They might be useful for mid to long-term weather forecasting.

3.7. Tropospheric temperature

Dobson et al. (1929) already realized that total column ozone is changing during the passage of tropospheric weather systems. This connection is relevant for interannual and longer time-scales as well (Steinbrecht et al., 1998). To account for it, tropospheric temperature (at 400 hPa), highly correlated with other parameters of tropospheric weather such as tropopause height, or temperature at other tropospheric levels, was included in the predictors of Eq. (1). The size of total ozone and 50 hPa (lower stratospheric) temperature variations correlated with (tropospheric) temperature at 400 hPa is given in Fig. 9. Nearly over the entire globe, high tropospheric temperature goes hand in hand with low total ozone and low temperature in the lower stratosphere. The corresponding variations are quite large and exceed 30 DU or 3 K at higher latitudes, north of 30° N or south of 40° S. In general, the seasonal dependence of these pattern is weak (not shown), although the largest amplitudes are found in spring, in the respective hemisphere. In the tropics, total ozone and lower stratospheric temperature variations correlated with 400 hPa temperature are smaller than at higher latitudes. They typically amount to less than 10 DU or 1 K. The geographical patterns look similar for total ozone and temperature. Also, observations and model simulations present a similar picture.

This strong negative correlation between tropospheric temperature and lower stratospheric ozone and temperature can be explained by up- and downward motions in the lower stratosphere, which compensate opposite vertical motions in the troposphere

(Steinbrecht et al., 1998; Labitzke and van Loon, 1999). In a tropospheric high pressure system, sinking air in the troposphere leads to adiabatic warming there. The tropopause and air in the lower stratosphere rise. This results in adiabatic cooling in the lower stratosphere and moves ozone poor air up. Total ozone decreases. A
5 tropospheric low pressure system has vertical motions in the opposite direction, and consequently a cold troposphere and a warm, ozone rich lower stratosphere with high total ozone. These vertical motions go hand in hand with horizontal advection, e.g. of ozone poor air from low latitudes, or of ozone rich air from high latitudes in the lower stratosphere (Salby and Callaghan, 1993; Koch et al., 2002). A typical low pressure
10 system advects ozone poor low-latitude air above its tropospheric warm sector, where the tropopause is high, and advects ozone rich high-latitude air above its tropospheric cold sector, where the tropopause is low. Salby and Callaghan (1993) estimate that vertical motions account for about two thirds, and horizontal advection for about one third of the total ozone fluctuations. Note that increased/decreased radiative heating
15 by more/less ozone also tends to give a positive correlation between total ozone and lower stratospheric temperature, especially on longer time-scales (Ramaswamy et al., 2001).

3.8. El Niño – Southern Oscillation

The El Niño – Southern Oscillation (ENSO) phenomenon of the tropical Pacific is one
20 of the major modes of variance for tropical sea-surface temperature and for the troposphere. The corresponding Southern Oscillation Index is plotted in Fig. 1. This index is positive during La Niña cold phases and negative during El Niño warm phases. The corresponding changes in tropical tropospheric temperature at 400 hPa can be seen in the bottom panel of Fig. 1.

25   To estimate the ENSO effect, the regression was done without including 400 hPa temperature as a predictor in Eq. (1). Note, however, that outside of the tropics, results would be very similar even if $T(400)$ would be included (see Steinbrecht et al., 2003). Figure 10 shows the typical size of total ozone and temperature changes between

EGU

La Niñas and El Niños for northern winter (December/January/February). Observations and model simulations show comparable features, especially for tropospheric temperature at 400 hPa. This has to be expected, since realistic sea surface temperatures are prescribed for the simulations.

Observed and simulated patterns are less comparable for total ozone and lower stratospheric temperature. Throughout much of the tropics, especially above the Eastern Pacific, total ozone and lower stratospheric temperature at 50 hPa are higher during La Niña, whereas tropospheric temperature is lower during La Niña. The difference is typically 5 to 15 DU, or 0.5 to 2 K, for total ozone and 50 hPa temperature respectively. These stratospheric changes have the opposite sign of the tropospheric variation, which can exceed 3 K in the tropical eastern Pacific, the region of the largest effect. Northern fall and spring (September/October/November, and March/April/May, both not shown) exhibit similar, but slightly weaker and less significant variations. In the summer hemisphere, i.e. December/January/February for the Southern Hemisphere, or June/July/August for the Northern Hemisphere (not shown), total ozone and 50 hPa temperature anomalies outside of the tropics have the opposite sign of the tropical anomalies. Both are generally lower during La Niña, and higher during El Niño. The extratropical response in the troposphere is largest in the Pacific area in winter, and its sign is also opposite to the tropics.

Observations/reanalyses and the two model simulations show comparable ENSO related patterns for 400 hPa temperature. For total ozone and 50 hPa temperatures, Fig. 10 shows some similarities, but also differences, e.g. in the a-zonal high latitude features, or in the Equatorial minimum of the 50 hPa temperature pattern, that occurs in the simulations, but not in NCEP reanalysis.

A striking zonally asymmetric feature, present in observations and simulations, are the substantially lower 50 hPa temperatures during La Niña over Eastern Asia or over the Aleutians/North America (−3 K, blue region in Fig. 10). Compared to the observations, the negative temperature anomaly over Eastern Asia is shifted east, towards the Aleutians or North America, in the models. A corresponding negative (blue) total ozone

ACPD

5, 9207–9248, 2005

Interannual variations of total ozone and temperature

W. Steinbrecht et al.

Title Page

Abstract | Introduction

Conclusions | References

Tables | Figures

◄ | ►

◄ | ►

Back | Close

Full Screen / Esc

Print Version

Interactive Discussion

EGU

anomaly does appear in both simulations, but not in the TOMS/SBUV data (or is not significant there). This large stratospheric feature near the Aleutians must be related to the tropospheric dipole feature of positive 400 hPa temperature anomalies above the Aleutians and negative anomalies above North America. This dipole is found both in

5   observations and simulations. The negative stratospheric pattern near the Aleutians is accompanied, in NCEP reanalysis and MAECHAM4-CHEM simulation, by a positive pattern of warmer 50 hPa temperatures and higher total ozone above Europe (up to +3 K, or +10 DU, red and yellow region).

These ENSO anomaly patterns near the Aleutians indicate changes in the Aleutian

10 tropospheric cyclone and stratospheric anti-cyclone that are correlated with ENSO. A generally stronger and more stable Arctic polar vortex during La Niña has been reported, e.g. in Labitzke and van Loon (1999). This is consistent with our findings, and has to be expected for the weaker Aleutian stratospheric anti-cyclone indicated by Fig. 10. Note, however, that a strong polar signal from ENSO is at least partly taken

15 over by the zonal wind at 60°N explanatory variable in Eq. (1). Coupling between ENSO, QBO, solar cycle and polar vortex strength is possible and even likely (Labitzke and van Loon, 1999). Zonal asymmetry (Callaghan and Salby, 2002) and the Aleutian stratospheric anti-cyclone seem to play a key role. However, this cannot be investigated with our simple linear regression method. A better approach and a separate and more

20 detailed study, as well as possibly longer time series, are needed to address these issues.

4. Conclusions

Multiple linear regression can be used to quantify major modes of the interannual variation of total ozone and lower stratospheric temperature, both from long-term observa-

25 tions/reanalysis, and from new realistic 1960 to 1999 simulations with the MAECHAM4-CHEM and E39/C chemistry climate models. Comparison of the derived interannual variation patterns substantially extends the model validation from only a simple valida-

EGU

tion of climatological means and variances.

For a large part of the globe, 60% or more of the variance can be explained by assuming that anomalies of total ozone, or temperature at 50 hPa, can be described as a simple linear superposition of predictors accounting for trend, QBO, solar cycle, polar
5   vortex strength, stratospheric aerosol loading, tropospheric temperature and ENSO. In the troposphere, and in large bands above the mid-latitude jet-streams, however, only a minor fraction of the variance can be accounted for in this way. Nevertheless, some interesting tropospheric variations appear to be connected to the strength of the stratospheric winter vortices, the solar cycle, or even the QBO, both in observations
10   and simulations. This might be important for long-term weather forecasting.

For the different explanatory variables, total ozone and 50 hPa temperature fluctuations range from about 5 DU or 0.5 K (two standard deviations of the corresponding time series term in Eq. (1)) to 50 DU or 5 K, respectively. Substantial changes come from the linear trend term, up to −30 DU or −1.5 K/decade. Large variations come
15   from terms related to polar vortex strength, up to 50 DU or 5 K, from tropospheric meteorology, up to 30 DU or 3 K, or from the QBO, up to 25 DU or 2.5 K. The 11-year solar cycle, generally less than 25 DU or 2.5 K, or ENSO, up to 15 DU or 1.5 K, are somewhat smaller contributors. A large but sporadic effect results from stratospheric aerosol, which has lead to warming up to 3 K at low latitudes and to ozone depletion
20   up to −40 DU at high latitudes after the 1991 Pinatubo eruption.

Magnitude and geographical patterns of the changes correlated with these predictors are generally similar for observations and simulations. Despite its restriction to altitudes below 30 km, E39/C reproduces the observed variations surprisingly well. As expected from its extended altitude range up to 80 km, and its better representation of
25   upper stratospheric and mesospheric processes like gravity waves, the MAECHAM4-CHEM simulation usually gives better agreement with the observations, especially for those variability patterns which include upper stratospheric/mesospheric processes. Examples are the link between SH polar vortex strength and total ozone variability, or the QBO. On the other hand, both models represent linear trend, solar cycle, or

Interannual variations of total ozone and temperature

W. Steinbrecht et al.

Title Page

Abstract	Introduction
Conclusions	References
Tables	Figures

Back   Close

Full Screen / Esc

Print Version

Interactive Discussion

EGU

Interannual variations of total ozone and temperature

W. Steinbrecht et al.

tropospheric influence patterns almost equally well.

At low latitudes, patterns are mostly zonally symmetric. At high latitudes, however, zonal symmetry is often broken. High latitude patterns seem to be wave-like with a change in intensity and/or location of the Aleutian stratospheric anti-cyclone in the Northern Hemisphere, or the Australian anti-cyclone in the Southern Hemisphere. While the simulations often reproduce the magnitude of these zonally non-symmetric patterns, they usually shift their location to different longitudes.

For the present study we are not adressing connections between polar vortex strength, 11-year solar cycle, phase of the QBO, and possibly El Niño (Labitzke and van Loon, 2000; Ruzmaikin and Feynman, 2002; Lee and Smith, 2003). We speculate that the zonally non-symmetric nature of the high-latitude atmosphere is essential for these connections, and that they might work through the Aleutian and Australian stratospheric anti-cyclones, and, possibly, their corresponding tropospheric cyclones. In the regression according to Eq. (1), the zonal wind anomalies $u(60N)$ and $u(60S)$ to a large degree account for the net variations correlated with polar vortex strength, due to whatever factor may be contributing to polar vortex strength. Still, very similar results are found, when only solar cycle, QBO and linear trend are allowed as explanatory variables in Eq. (1), and the other explanatory variables are not used. Steinbrecht et al. (2003) showed results for the solar cycle effect during QBO westerly and QBO easterly phases, but the differences were not major. Similar results are also found in the model simulations, but are not shown here. Nevertheless, the whole issue is more complex, and merits a separate investigation in the future.

Both model simulations give a generally good representation of the variation of the atmosphere over the last 40 years. Unfortunately they both end in 1999. It will be very worthwile to extend these simulations to the present and into the future. Additional simulations, e.g. with individual influences switched on or off, will bring most valuable contributions to questions regarding the expected recovery of the stratospheric ozone layer, effects of climate change on stratosphere and troposphere, and to our understanding of the connections between these issues and between these different parts of

our atmosphere.

References

Austin, J., Shindell, D., Beagley, S. R., Brühl, C., Dameris, M., Manzini, E., Nagashima, T., Newman, P., Pawson, S., Pitari, G., Rozanov, E., Schnadt, C., and Shepherd, T. G.: Uncertainties and assessments of chemistry-climate models of the stratosphere, Atmos. Chem. Phys., 3, 1–27, 2003,
SRef-ID: 1680-7324/acp/2003-3-1. 9209, 9213, 9218, 9225

Baldwin, M. P., Gray, L. J., Dunkerton, T. J., Hamilton, K., Haynes, P. H., Randel, W. J., Holton, J. R., Alexander, M. J., Hirota, I., Horinouchi, T., Jones, D. B. A., Kinnersley, J. S., Marquardt, C., and Takahashi, M.: The Quasi-Biennial Oscillation, Rev. Geophys., 39, 179–229, 2001. 9220

Baldwin, M. P. and Dunkerton, T. J.: Propagation of the Arctic Oscillation from the stratosphere to the troposphere, J. Geophys. Res., 104, 30 937–30 946, 1999. 9225

Callaghan, P. F. and Salby, M. L.: Three-Dimensionality and forcing of the Brewer-Dobson circulation, J. Atmos. Sci., 59, 976–991, 2002. 9229

Dameris, M., Grewe, V., Ponater, M., Deckert, R., Eyring, V., Mager, F., Matthes, S., Schnadt, C., Stenke, A., Steil, B., Brühl, C., and Giorgetta, M. A.: Long-term changes and variability in a transient simulation with a chemistry-climate model employing realistic forcing, Atmos. Chem. Phys., 5, 2121–2145, 2005,
SRef-ID: 1680-7324/acp/2005-5-2121. 9209, 9210, 9211

Dobson, G. M. B., Harrison, D. N., and Lawrence, J.: Measurements of the amount of ozone in the earth's atmosphere and its relation to other geophysical conditions, III, Proc. Roy. Soc. London A, 122, 456–486, 1929. 9226

Fioletev, V. E., Bodeker, G. E., Miller, A. J., McPeters, R. D., and Stolarski, R.: Global and zonal total ozone variations estimated from ground-based and satellite measurements: 1964-2000, J. Geophys. Res., 107, 4647, doi:10.1029/2001JD001350, 2002. 9219

Title Page

Abstract | Introduction

Conclusions | References

Tables | Figures

◄ | ►►

◄ | ►

Back | Close

Full Screen / Esc

Print Version

Interactive Discussion

EGU

Giorgetta, M. A. and Bengtsson, L.: The potential role of the quasi-biennial oscillation in the stratosphere-troposphere exchange as found in water vapour in general circulation model experiments, J. Geophys. Res., 104, 6003–6019, 1999. 9211, 9220

Giorgetta, M. A., Manzini, E., and Roeckner, E.;, Forcing of the quasi-biennial oscillation from a broad spectrum of atmospheric waves, Geophys. Res. Lett., 29(D8), 1245, doi:10.1029/2002GL014756, 2002. 9220

Grewe, V., Brunner, D., Dameris, M., Grenfell, J. L., Hein, R., Shindell, D., and Staehelin, J.: Origin and variability of upper tropospheric nitrogen oxides and ozone at northern midlatitudes, Atmos. Environ., 35, 3421–3433, 2001. 9211

Grewe, V., Dameris, M., Fichter, C., and Sausen, R.: Impact of aircraft NO_x emissions. Part 1: Interactively coupled climate-chemistry simulations and sensitivities to climate-chemistry feedback, lightning and model resolution, Meteorol. Z., 3, 177–186, 2002. 9218

Hein, R., Dameris, M., Schnadt, C., Land, C., Grewe, V., Köhler, I., Ponater, M., Sausen, R., Steil, B., Landgraf, J., and Brühl, C.: Results of an interactively coupled atmospheric chemistry general circulation model: Comparison with observations, Ann. Geophys., 19, 435–457, 2001,
SRef-ID: 1432-0576/ag/2001-19-435. 9209

IPCC – Intergovernmental Panel on Climate Change: Climate Change 2001: The Scientific Basis, Contribution of Working Group I to the Third Assessment, Report of the Intergovernmental Panel on Climate Change (IPCC), edited by: Houghton, J. T., Ding, Y., Griggs, D. J., Noguer, M., van der Linden, P. J., and Xiaosu, D., Cambridge University Press, Cambridge, UK, 944 pp., 2001. 9209, 9219

Kistler, R., Kalnay, E., Collins, W., Saha, S., White, G., Woollen, J., Chelliah, M., Ebisuzaki, W., Kanamitsu, M., Kousky, V., van den Dool, H., Jenne, R., and Fiorino, M.: The NCEP-NCAR 50-Year Reanalysis: Monthly Means, CD-ROM and Documentation, Bull. Am. Met. Soc., 82, 247–267, http://www.cpc.ncep.noaa.gov/products/wesley/reanalysis.html, 2001. 9210, 9211

Koch, G., Wernli, H., Staehelin, J., and Peter, T.: A Lagrangian analysis of stratospheric ozone variability and long-term trends above Payerne (Switzerland) during 1970–2001, J. Geophys. Res., 107, 4373, doi:10.1029/2001JD001550, 2002. 9227

Labitzke, K. and van Loon, H.: The stratosphere: phenomena, history, and relevance, Springer Verlag, Berlin, 197 pp., 1999. 9227, 9229

Labitzke, K. and van Loon, H.: The QBO effect on the solar signal in the global stratosphere

EGU

in the winter of the Northern Hemisphere, J. Atmos. Solar-Terr. Phys., 62, 621–628, 2000. 9231

Lean, J. L., Rottman, G. J., Kyle, H. L., Woods, T. N., Hickey, J. R., and Puga, L. C.: Detection and parameterization of variations in solar mid- and near-ultraviolet radiation (200–400 nm), J. Geophys. Res., 102, 29 939–29 956, 1997. 9211

Lee, H. and Smith, A. K.: Simulation of the combined effects of solar cycle, quasi-biennial oscillation, and volcanic forcing on stratospheric ozone changes in recent decades, J. Geophys. Res., 108(D2), 4049, doi:10.1029/2001JD001503, 2003. 9231

Manzini, E. and Bengtsson, L.: Stratospheric climate and variability from a general circulation model and observations, Clim. Dynam., 12 , 615–639, 1996. 9210, 9211

Manzini, E. and McFarlane, N. A.: The effect of varying the source spectrum of a gravity wave parameterization in a middle atmosphere general circulation model, J. Geophys. Res., 103, 31 523–31 539, 1998. 9211

Manzini, E., Steil, B., Brühl, C., Giorgetta, M. A., and Krüger, K.: A new interactive chemistry climate model: 2. Sensitivity of the middle atmosphere to ozone depletion and increase in greenhouse gases and implications for recent stratospheric cooling, J. Geophys. Res., 108(D14), 4429, doi:10.1029/2002JD002977, 2003. 9209, 9211

Newchurch, M. J., Yang, E.-S., Cunnold, D. M., Reinsel, G. C., Zawodny, J. M., and Russell III, J. M.: Evidence for slowdown in stratospheric ozone loss: First stage of ozone recovery, J. Geophys. Res., 108(D16), 4507, doi:10.1029/2003JD003471, 2003. 9219

Ramaswamy, V., Chanin, M. L., Angell, J., Barnett, J., Gaffen, D., Gelman, M., Keckhut, P., Koshelkov, Y., Labitzke, K., Lin, J. J. R., O'Neil, A., Nash, J., Randel, W., Rood, R., Shiotani, M., Swinbank, R., and Shine, K.: Stratospheric temperature trends: observations and model simulations, Rev. Geophys., 39, 71–122, 2001. 9219, 9227

Rasch, P. J. and Lawrence, M. G.: Recent developments in transport methods at NCAR, in: Proceedings of the MPI workshop on conservative transport methods, Report No. 265, edited by: Machenhauer, B., 93 pp., Max Planck Institute for Meteorology, Hamburg, Germany, 1998. 9211

Rayner, N. A., Parker, D. E., Horton, E. B., Folland, C. K., Alexander, L. V., Rowell, D. P., Kent, E. C., and Kaplan, A.: Global analyses of sea surface temperature, sea ice, and night marine air temperature since the late nineteenth century, J. Geophys. Res., 108(D14), 4407, doi:10.1029/2002JD002670, 2003. 9211

Rinsland, C. P., Mahieu, E., Zander, R., Jones, N. B., Chipperfield, M. P., Goldman, A., An-

Interannual variations of total ozone and temperature

W. Steinbrecht et al.

Title Page

Abstract	Introduction
Conclusions	References
Tables	Figures

|◄ | ►|
◄ | ►

Back | Close

Full Screen / Esc

Print Version

Interactive Discussion

EGU

derson, J., Russell III, J. M., Demoulin, P., Notholt, J., Toon, G. C., Blavier, J.-F., Sen, B., Sussmann, R., Wood, S. W., Meier, A., Griffith, D. W. T., Chiou, L. S., Murcray, F. J., Stephen, T. M., Hase, F., Mikuteit, S., Schulz, A., and Blumenstock, T.: Long-term trends of inorganic chlorine from ground-based infrared solar spectra: Past increases and evidence for stabi-
5   lization, J. Geophys. Res., 108(D8), 4252, doi:10.1029/2002JD003001, 2003. 9219

Robock, A.: Volcanic eruptions and climate, Rev. Geophys., 38, 191–219, 2000. 9222, 9223

Roeckner, E., Arpe, L., Bengtsson, L., Christoph, M., Claussen, M., Dümenil, L., Esch, M., Giorgetta, M. A., Schlese, U., and Schulzweida, U.: The atmospheric general circulation model ECHAM-4: Model description and simulation of present-day climate, Rep. No. 218,
10   MPI-Meteorologie, Hamburg, Germany, 90 pp., 1996. 9210

Ruzmaikin, A. and Feynman, J.: Solar influence on a major mode of atmospheric variability, J. Geophys. Res., 107(D14), doi:10.1029/2001JD001239, 2002. 9231

Salby, M. L. and Callaghan, P. F.: Fluctuations of total ozone and their relationship to strato-spheric air motions, J. Geophys. Res., 98, 2715–2727, 1993. 9227

15   Salby, M. L. and Callaghan, P. F.: Interannual changes of the stratospheric circulation: relation-ship to ozone and tropospheric structure, J. Clim., 24, 3673–3685, 2002. 9224

Schnadt, C., Dameris, M., Ponater, M., Hein, R., Grewe, V., and Steil, B.: Interaction of at-mospheric chemistry and climate and its impact on stratospheric ozone, Clim. Dyn., 18, 501–517, 2002. 9211

20   Schnadt, C. and Dameris, M.: Relationship between North Atlantic Oscillation changes and stratospheric ozone recovery in the Northern Hemisphere in a chemistry-climate model, Geophys. Res. Lett., 30(9), 1487, doi:10.1029/2003GL017006, 2003. 9211

Shine, K. P., Bourqui, M. S., Forster, P. M. F., Hare, S. H. E., Langematz, U., Braesicke, P., Grewe, V., Ponater, M., Schnadt, C., Smith, C. A., Haigh, J. D., Austin, J., Butchart, N.,
25   Shindell, D. T., Randel, W. J., Nagashima, T., Portmann, R. W., Solomon, S., Seidel, D. J., Lanzante, J., Klein, S., Ramaswamy, V., and Schwarzkopf, M. D.: A comparison of mod-elsimulated trends in stratospheric temperatures, Quart. J. R. Met. Soc., 129, 1565–1588, 2003. 9209, 9219

Solomon, S., Portmann, R. W., Garcia, R. R., Thomason, L. W., Poole, L. R., and McCormick,
30   M. P.: The role of aerosol variations in anthropogenic ozone depletion at northern midlati-tudes, J. Geophys. Res., 101, 6713–6727, 1996. 9223

Solomon, S.: Stratospheric ozone depletion: A review of concepts and history, Rev. Geophys., 37, 275–316, 1999.

Steil, B., Dameris, M., Brühl, C., Crutzen, P. J., Grewe, V., Ponater, M., and Sausen, R.: Development of a chemistry module for GCMs: first results of a multiannual integration, Ann. Geophys., 16, 205–228, 1998, SRef-ID: 1432-0576/ag/1998-16-205. 9210

5 Steil, B., Brühl, C., Manzini, E., Crutzen, P. J., Lelieveld, J., Rasch, P. J., Roeckner, E., and Krüger, K.: A new interactive chemistry climate model: 1. Present day climatology and interannual variability of the middle atmosphere using the model and 9 years of HALOE/UARS data, J. Geophys. Res., 108(D9), 4290, doi:10.1029/2002JD002971, 2003. 9209, 9210, 9211, 9218

10 Steinbrecht, W., Claude, H., Köhler, U., and Hoinka, K. P.: Correlations between tropopause height and total ozone: Implications for long-term changes, J. Geophys. Res., 103, 19 183–19 192, 1998. 9226, 9227

Steinbrecht, W., Hassler, B., Claude, H., Winkler, P., and Stolarski, R. S.: Global distribution of total ozone and lower stratospheric temperature variations, Atmos. Chem. Phys., 3, 1421–

15 1438, 2003, SRef-ID: 1680-7324/acp/2003-3-1421. 9210, 9215, 9219, 9231

Steinbrecht, W., Claude, H., and Winkler, P.: Enhanced upper stratospheric ozone: Sign of recovery or solar cycle effect?, J. Geophys. Res., 109(D2), 2308, doi:10.1029/2003JD004284, 2004. 9219

20 Stenke, A. and Grewe, V.: Simulation of stratospheric water vapour trends: impact on stratospheric chemistry, Atmos. Chem. Phys., 5, 1257–1272, 2005, SRef-ID: 1680-7324/acp/2005-5-1257. 9223

Stolarski, R. S. and Hollandsworth-Frith, S.: Combined total ozone record from TOMS and SBUV instruments, http://code916.gsfc.nasa.gov/Data_services/merged/data/toms_sbuv.v3.

25 78-02.5x10.v7.txt, 2003. 9210, 9211

Timmreck, C., Graf, H.-F., and Steil, B.: Aerosol chemistry interactions after the Mt. Pinatubo eruption, in: Volcanism and the Earth's Atmosphere, edited by: Robock, A. and Oppenheimer, C., Geophys. Monograph Series, 139, American Geophysical Union, Washington D.C., pp. 213–225, 2004. 9211, 9223

30 Thompson, D. W. J. and Wallace, J. M.: Annular modes in the extratropical circulation. Part I: Month-to-month variability, J. Climate, 13, 1000–1016, 2000. 9225

Tourpali, K., Schuurmans, C. J. E., van Dorland, R., Steil, B., and Brühl, C.: Stratospheric and tropospheric response to enhanced solar UV-radiation: A model study, Geophys. Res. Lett.,

Interannual variations of total ozone and temperature

W. Steinbrecht et al.

Title Page

Abstract	Introduction
Conclusions	References
Tables	Figures

◄ | ►│

◄ | ►

Back | Close

Full Screen / Esc

Print Version

Interactive Discussion

EGU

30(5), 1231, doi:10.1029/2002GL016650, 2003. 9211, 9222

Tourpali, K., Schuurmans, C. J. E., van Dorland, R., Steil, B., Brühl, C., and Manzini, E.: Solar cycle modulation of the North Atlantic Oscillation in a Chemistry-Climate Model, Geophys. Res. Lett., 32(17), L17803, doi:10.1029/2005GL023509, 2005. 9222

5 Williamson, D. L. and Rasch, P. J.: Two-dimensional semi-Lagrangian transport with shape preserving interpolation, Mon. Wea. Rev., 117, 102–129, 1989. 9211

WMO (World Meteorological Organization): Scientific Assessment of Ozone Depletion: 2002, Global Ozone Research and Monitoring ProjectReport No. 47, 498 pp., Geneva, http://www.wmo.ch/web/arep/ozone.html, 2003. 9209, 9219

10 Yang, H. and Tung, K. K.: On the phase propagation of extra tropical Quasi-Biennial Oscillation in observational data, J. Geophys. Res., 100, 9091–9100, 1995. 9220

Interannual variations of total ozone and temperature
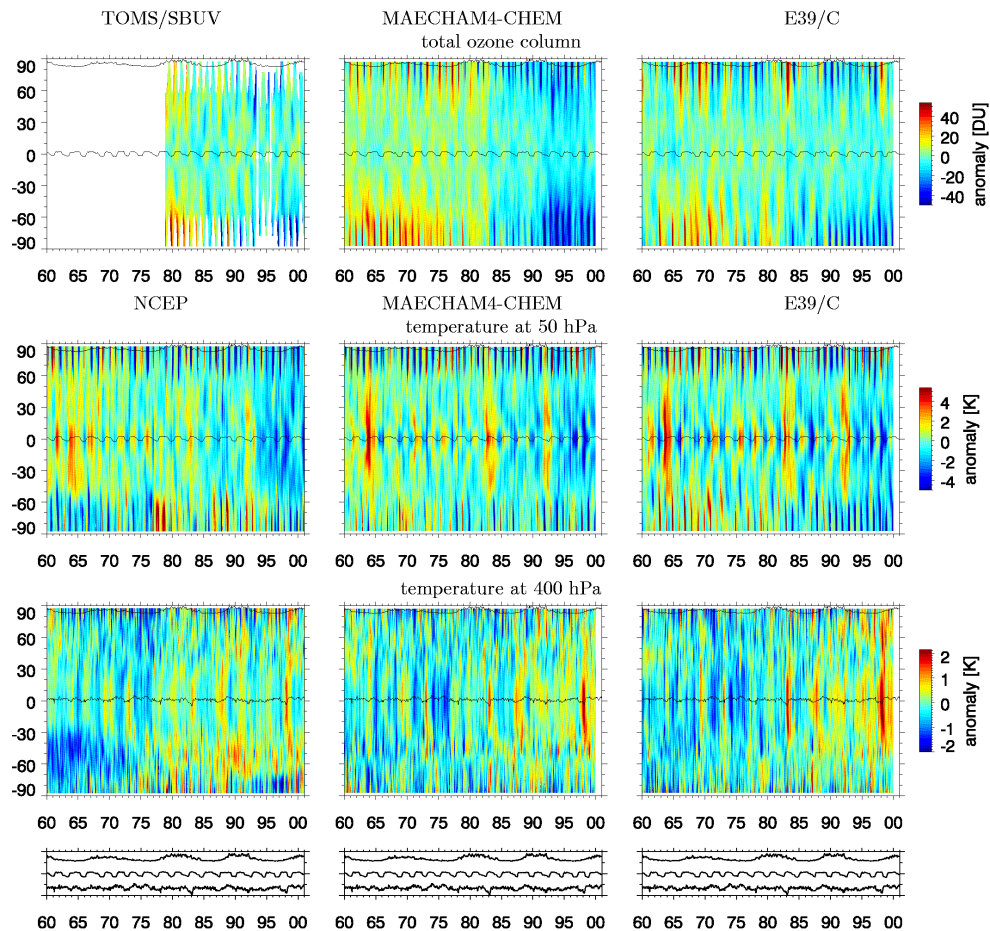
W. Steinbrecht et al.

Title Page

Abstract	Introduction
Conclusions	References
Tables	Figures

◀ | ▶|

◀ | ▶

Back | Close

Full Screen / Esc

Print Version

Interactive Discussion

EGU

Fig. 1.

Title Page

Abstract | Introduction

Conclusions | References

Tables | Figures

◀ | ▶

◀ | ▶

Back | Close

Full Screen / Esc

Print Version

Interactive Discussion

EGU

EGU

Fig. 1. Zonal anomaly time series for latitudes from 90° S to 90° N (y-axes), and for the period 1960 to 2000 (x-axes). Anomalies are color-coded with yellow and red colours corresponding to positive anomalies, and cyan and blue colors corresponding to negative anomalies. Top row shows total column ozone anomalies, next row temperature anomalies at 50 hPa (≈22 km), and next row temperature anomalies at 400 hPa (≈7 km). The left column gives results for TOMS/SBUV observations, not available before 1979, and for NCEP reanalysis, the middle column for the transient simulation with MAECHAM4-CHEM, and the right column for the transient simulation with ECHAM4.L39(DLR)/CHEM (=E39/C). The black line near the top of each plot gives 10.7 cm solar-flux as an indicator for the 11-year solar cycle. The black line near the Equator in the two top rows gives equatorial zonal wind anomalies at 40 hPa as a proxy for the QBO. In the third row, the black line near the Equator gives the Southern Oscillation Index, which is negative during El Niño warm events and positive during La Niña cold events. At the very bottom, these three index time series are repeated again.
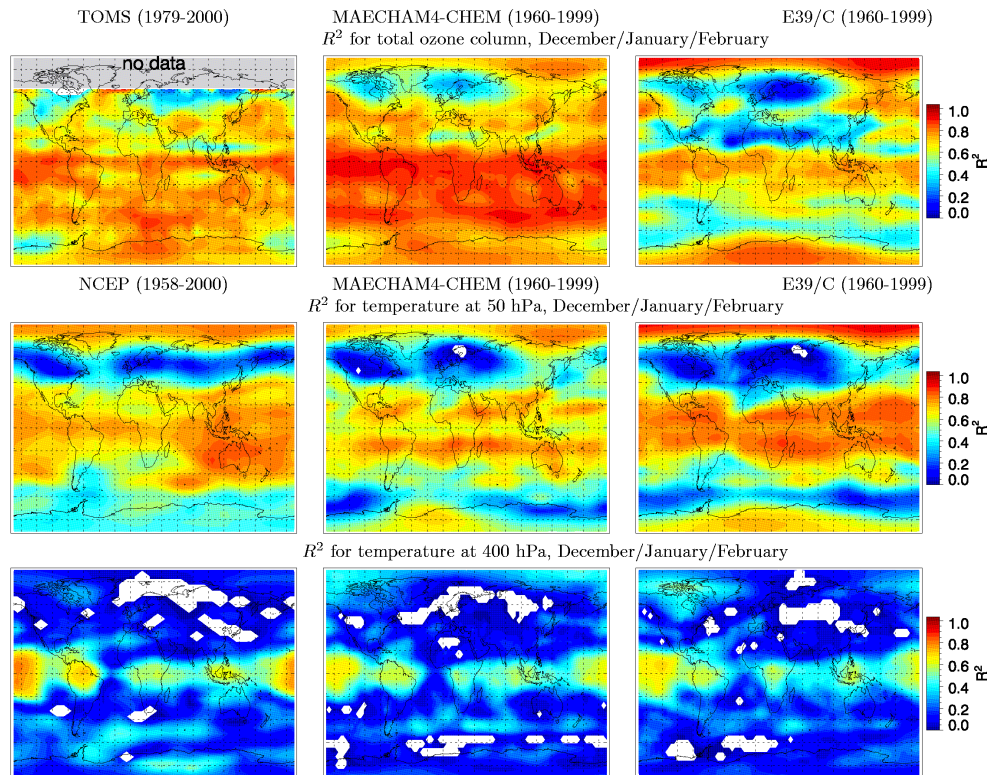
Fig. 2. Global maps of R^2 for northern winter (December/January/February). Top row gives results for total ozone anomalies, middle row results for temperature anomalies at 50 hPa ($\approx$22 km), and bottom row results for temperature anomalies at 400 hPa ($\approx$7 km). R^2 for TOMS/SBUV observations and NCEP reanalyses results is given in the left column, R^2 for the MAECHAM4-CHEM transient simulation in the middle column, and R^2 for the ECHAM4.L39(DLR)/CHEM (=E39/C) transient simulation in the right column. TOMS/SBUV observations are not available before 1979 and are not available in polar regions in winter (grey area).
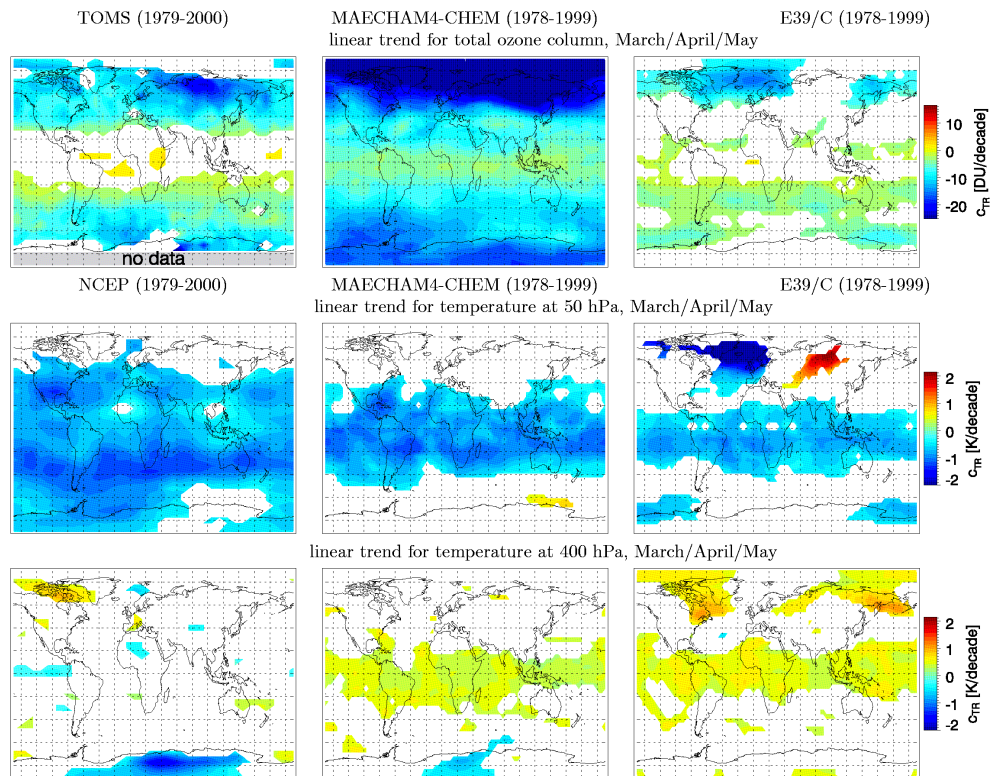
Fig. 3. Similar to previous figure, but showing the linear trend coefficient for northern spring (March/April/May). Top panels give the total ozone trend coefficient in DU per decade, middle and bottom panels give the temperature trend coefficient in K per decade, for 50 hPa ($\approx$22 km) and 400 hPa ($\approx$7 km), respectively. The time period is 1979 to 2000 for observations/reanalysis in the left panels, and is 1978 to 1999 for the model runs in the middle and right panels. In the white regions the linear trend term is not statistically significant at the 90% confidence level.

ACPD

5, 9207–9248, 2005

Interannual variations of total ozone and temperature

W. Steinbrecht et al.

Title Page

Abstract | Introduction

Conclusions | References

Tables | Figures

I◀ | ▶I

◀ | ▶

Back | Close

Full Screen / Esc

Print Version

Interactive Discussion

EGU
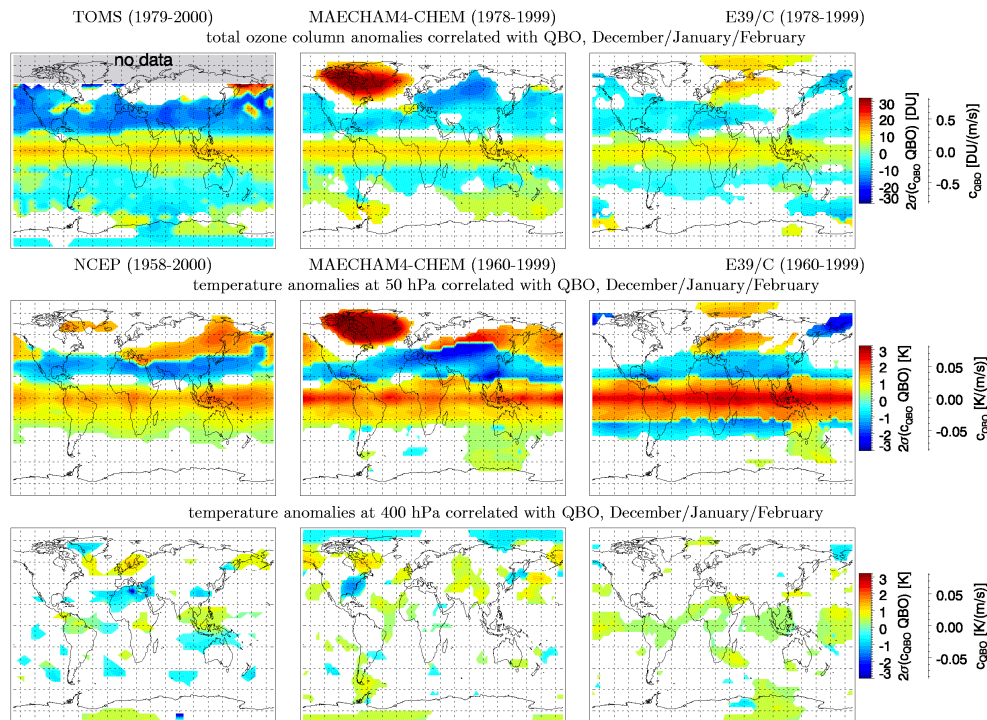
Fig. 4. Similar to previous figure, but showing two standard deviations (2σ) of the combined QBO term in the regression, for northern winter (December/January/February). The second scales, on the right, give the approximate size of the QBO regression coefficient $\sqrt{c^2_{QBO(10)} + c^2_{QBO(30)}}$. Blue colors indicate inverse (negative) correlation with westerly zonal wind at 30 hPa at the Equator, whereas yellow and red colors indicate positive correlation. For total ozone in the top panels a shorter time period is considered. White regions have no statistically significant QBO-related variation, at the 90% confidence level.

W. Steinbrecht et al.

Title Page	
Abstract	Introduction
Conclusions	References
Tables	Figures
◄◄	►►
◄	►
Back	Close

Full Screen / Esc

Print Version

Interactive Discussion

EGU
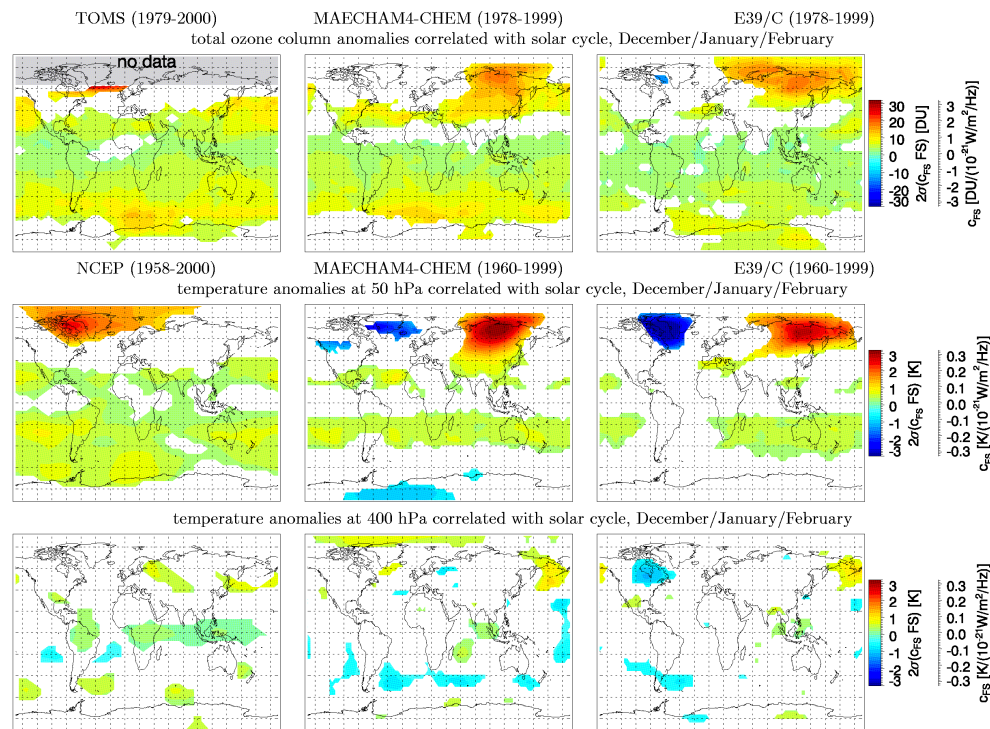
Fig. 5. Same as Fig. 4, but for the size (2σ) of total ozone and temperature anomalies associated with the 11-year solar cycle. The scales on the false color bars give 2 standard deviations (2σ) of the solar cycle term $c_{FS} FS$ in Eq. (1). The second scales give the size of the solar cycle regression coefficient c_{FS}. Yellow and red colors indicate positive correlation between total ozone and solar flux.

Interannual variations of total ozone and temperature

W. Steinbrecht et al.

EGU
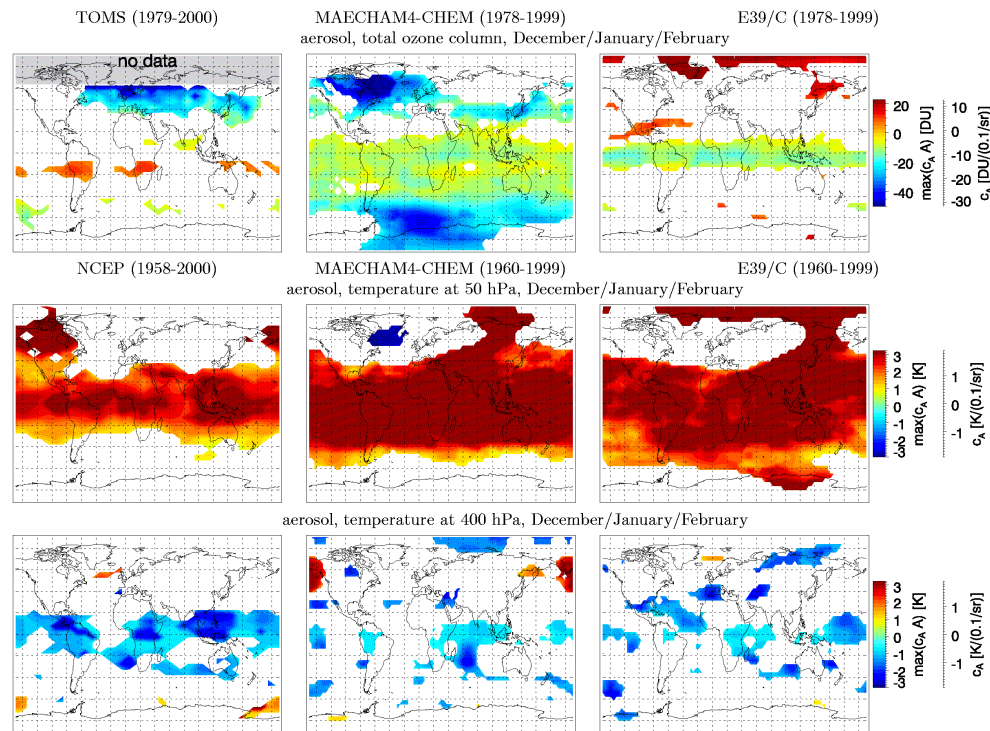
Fig. 6. Similar to previous figures, but for anomalies attributed to stratospheric aerosol from volcanic eruptions, mostly the Mt. Pinatubo eruption. Here the maximum positive or negative anomalies due to the aerosol term ($c_A A$) are shown, not two standard deviations as in the other plots. Red and yellow colors denote positive anomalies, cyan and blue colors negative anomalies. Note that the scale for c_A on the right is only approximate, because aerosol optical density A varies with latitude.

Interannual variations of total ozone and temperature

W. Steinbrecht et al.

[EGU](#)

TOMS (1979-2000) MAECHAM4-CHEM (1978-1999) E39/C (1978-1999)
total ozone column anomalies correlated with zonal wind anomalies at 60°N, 50 hPa, March/April/May

NCEP (1958-2000) MAECHAM4-CHEM (1960-1999) E39/C (1960-1999)
temperature anomalies at 50 hPa correlated with zonal wind anomalies at 60°N, 50 hPa, March/April/May

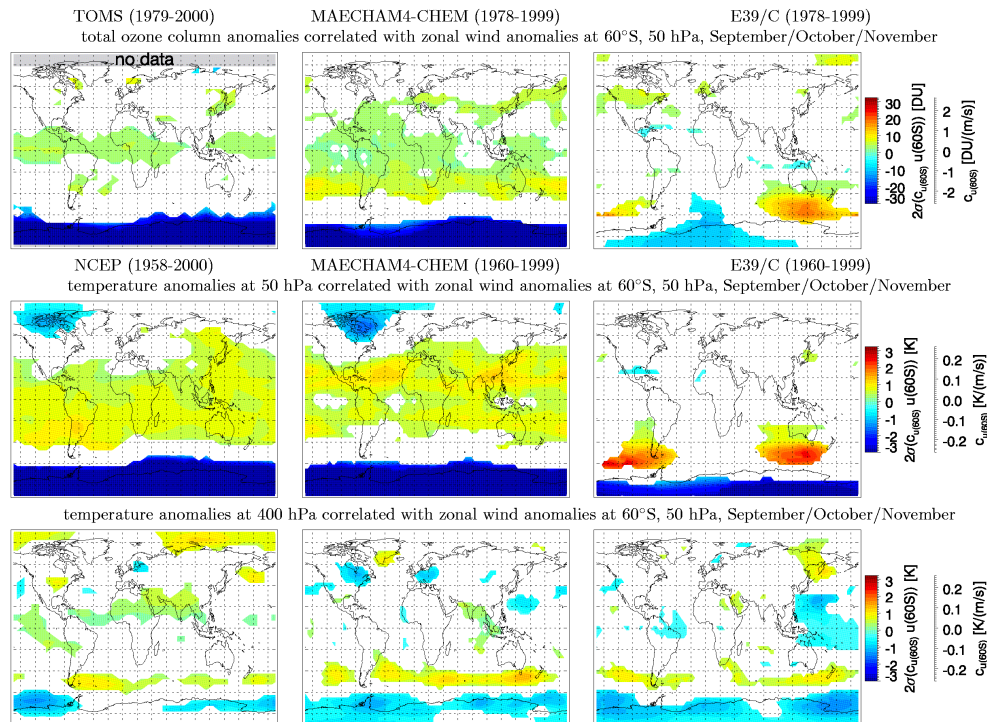temperature anomalies at 400 hPa correlated with zonal wind anomalies at 60°N, 50 hPa, March/April/May
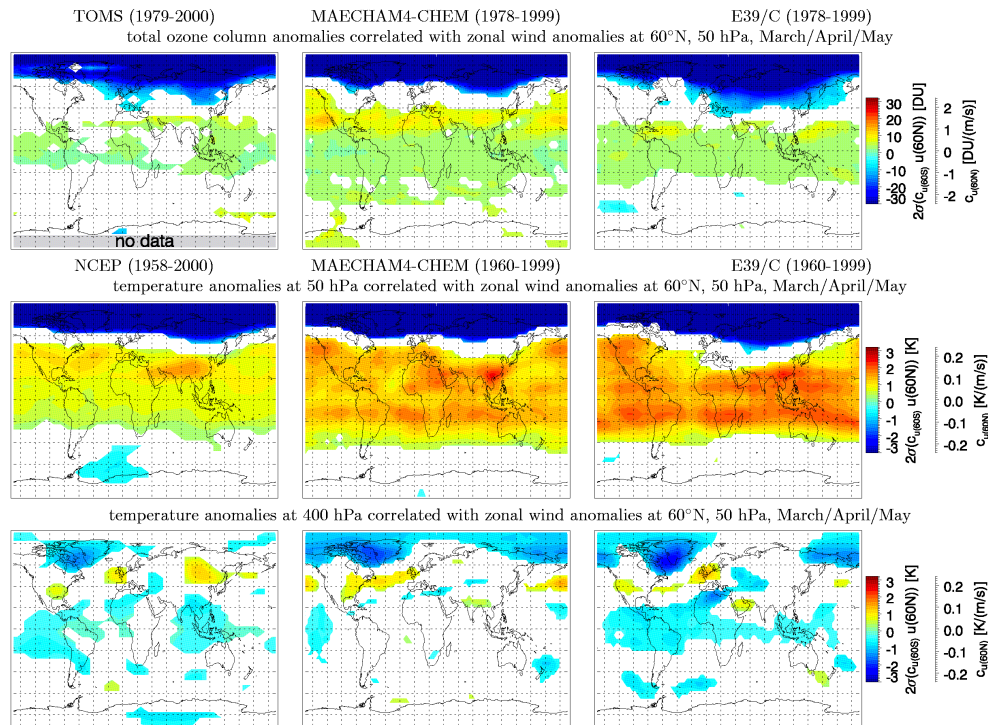
Fig. 7. Similar to previous figures, but showing the size (2σ) of anomalies related to Arctic polar vortex strength, for northern spring (March/April/May). Polar vortex strength is represented by zonal wind anomalies at 60° N, 50 hPa.

Interannual variations of total ozone and temperature

W. Steinbrecht et al.

TOMS (1979-2000) MAECHAM4-CHEM (1978-1999) E39/C (1978-1999)
total ozone column anomalies correlated with zonal wind anomalies at 60°S, 50 hPa, September/October/November

NCEP (1958-2000) MAECHAM4-CHEM (1960-1999) E39/C (1960-1999)
temperature anomalies at 50 hPa correlated with zonal wind anomalies at 60°S, 50 hPa, September/October/November

temperature anomalies at 400 hPa correlated with zonal wind anomalies at 60°S, 50 hPa, September/October/November

Fig. 8. Same as Fig. 7, but for Antarctic polar vortex strength, and southern spring (September/October/November). Antarctic polar vortex strength is represented by zonal wind anomalies at 60° S, 50 hPa.

Interannual variations of total ozone and temperature

W. Steinbrecht et al.

EGU
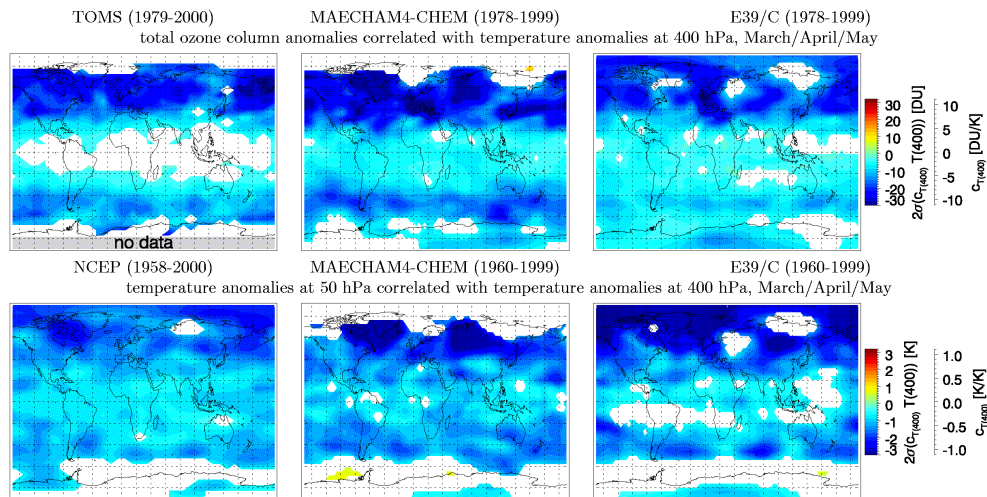
Fig. 9. Similar to previous figures, but showing the size (2σ) of stratospheric ozone and 50 hPa temperature anomalies attributed to tropospheric temperature anomalies at 400 hPa (term $c_{T(400)}T(400)$). The second scales, on the right, only give the approximate size of the regression coefficient $c_{T(400)}$.

Interannual variations of total ozone and temperature

W. Steinbrecht et al.

EGU
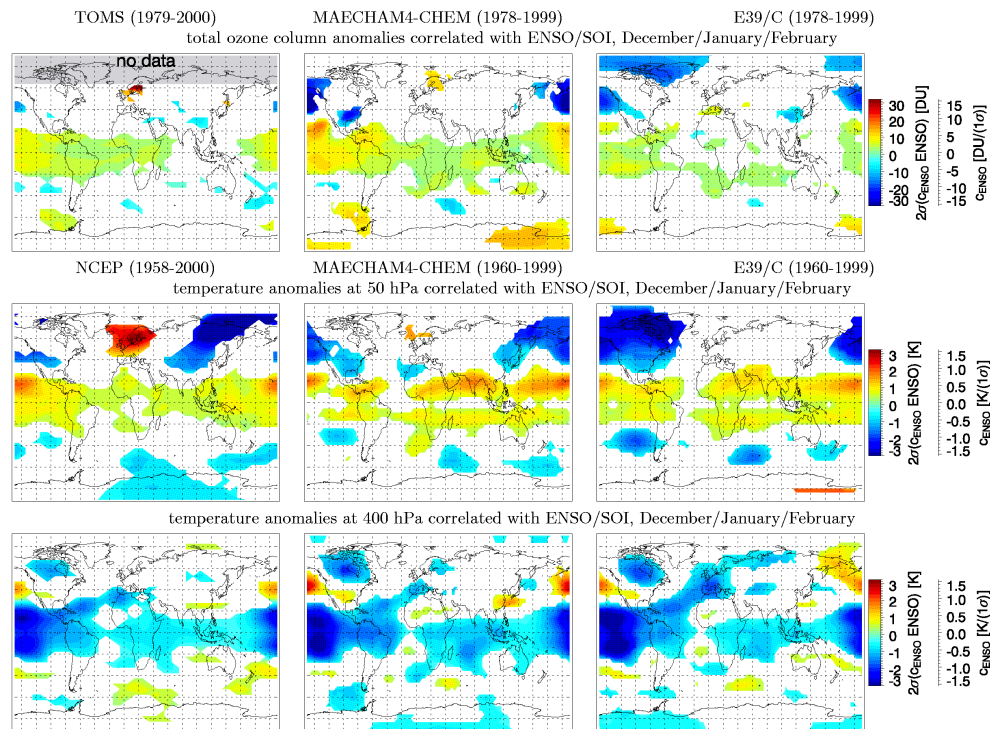
Fig. 10. Same as previous figures, but showing the size (2σ) of anomalies correlated with the El Niño Southern-Oscillation Index. These results where obtained without using 400 hPa temperature as an explanatory variable in Eq. (1).